Trends in $4d$-subshell photoabsorption along the iodine isonuclear sequence: I, I^+, and I^{2+}

G. O'Sullivan,[1] C. McGuinness,[1] J. T. Costello,[2] E. T. Kennedy,[2] and B. Weinmann[1]
[1]*Physics Department, University College Dublin, Belfield, Dublin 4, Ireland*
[2]*School of Physical Sciences, Dublin City University, Glasnevin, Dublin 9, Ireland*
(Received 21 July 1995)

The $4d$ absorption spectra of I, I^+, and I^{2+} have been observed in the 45–300-eV region using the dual laser-produced plasma technique. At lower energies each spectrum is dominated by intense $4d\rightarrow 5p$ transitions, which are identified with the aid of multiconfiguration Hartree-Fock calculations. The excited states decay by direct autoionization involving $5s$ or $5p$ electrons and rates for the different processes and resulting linewidths were calculated and compared, where possible, with experiment. In the case of neutral iodine $4d\rightarrow 6p$ transitions are also observed in the region close to the $^2D_{5/2}$ threshold. The dominant feature in each spectrum, however, arises from $4d$-f excitation, which evolves from a $4d$-εf shape resonance in neutral iodine to a feature containing discrete $4d\rightarrow nf$ transitions in I^{2+}.

PACS number(s): 32.80.Hd, 32.30.Jc, 52.50.Jm

I. INTRODUCTION

In the past, the advantage of using the dual laser-produced plasma (DLP) method for the investigation of the inner-shell absorption spectra of refractory atoms as well as its applicability to the study of photoabsorption in metallic ions has been highlighted in a number of experiments [1,2]. Now it is shown that instead of using pure metallic targets, compressed salts containing halogen or chalcogen atoms may be substituted and the spectra of these species readily obtained. Moreover, this technique may be used for studies on any element that is chemically reactive, gaseous or liquid, or otherwise difficult to isolate or contain under the experimental conditions normally obtaining in the extreme-ultraviolet (XUV) region. In the present experiment the target material used was KI, as the potassium spectrum has only a few strong features in the 45–300-eV region and these could be readily distinguished by comparison with spectra from a KBr target. The conventional method of producing iodine atoms is flash photolosis [3] or laser-induced photodissociation of I_2 [4,5] in which 95% photodissociation into the ground $^2P_{3/2}$ level has been achieved [6–8] and which has permitted the investigation of the $4d$ excitation and decay dynamics of neutral iodine. In these experiments the spectrum was found to be dominated by intense $4d\rightarrow 5p$ transitions which decay primarily by direct autoionization into outer-shell channels because of the valence character of the $5p$ orbital [6]. In contrast, in the case of rare gases for which the first empty orbital has a Rydberg character the dominant relaxation mechanism is a resonant Auger process in which the promoted electron remains as a spectator or is involved in a shake process [9]. Such a scenario has also been observed for the decay of the $4d^9 5p^5 6p$ states of iodine [7]. However, the dominant feature is the $4d$-εf shape resonance above the $4d$ ionization threshold ionization which originates (in the single-electron picture) from the interaction of the escaping photoelectron and the $l=3$ centrifugal barrier which causes the total potential to have two minima, one at small r containing no bound states and one at large r which is effectively hydrogenic in character and contains the nf Rydberg levels [10]. This shape resonance is weaker in iodine than in Xe or higher-Z elements and the hole state decays preferentially into I^{2+} and I^{3+} by Auger processes reflecting the continuum nature of the εf state [8]. No equivalent data exist for excitation processes in iodine ions because of the difficulty in preparing a suitable ion population for backlighting with synchrotron radiation.

In the present paper our experimental results for the $4d\rightarrow 5p$ and $6p$ spectra of neutral iodine are compared with earlier data and the results of atomic structure calculations. This comparison provides a calibration of the theory which is then used to identify the $4d\rightarrow 5p$ spectra of I^+ and I^{2+} and to make predictions for the decay pathways available to these autoionizing states. Our $4d\rightarrow 4f$ spectrum of neutral iodine is then compared to the earlier experimental and theoretical data and calculations performed here within both single-particle and many-body frameworks. These calculations are then extended to I^+ and I^{2+} and compared with the experimental data for these ions.

II. EXPERIMENT

The experimental arrangement has already been described elsewhere [11,12]. Spectra were recorded both photographically and photoelectrically. Photographic recording has the advantage of broad energy coverage and high-energy resolution for sharp discrete features but it is generally less suitable for recording the profiles of broad autoionizing resonances and continuum features because of the nonlinearity of the photographic response and saturation effects. Photoelectric recording gives more limited energy coverage and resolution but excels for obtaining profiles and line-shape data because of its superior response both in terms of dynamic range and linearity. A 1-J, 30-ns Q-switched ruby laser pulse was focused onto a salt target which had been compressed to form a pellet to yield a plasma column containing ionized iodine. In the photographic work, focusing is achieved through a crossed cylindrical lens assembly which yields a 200-

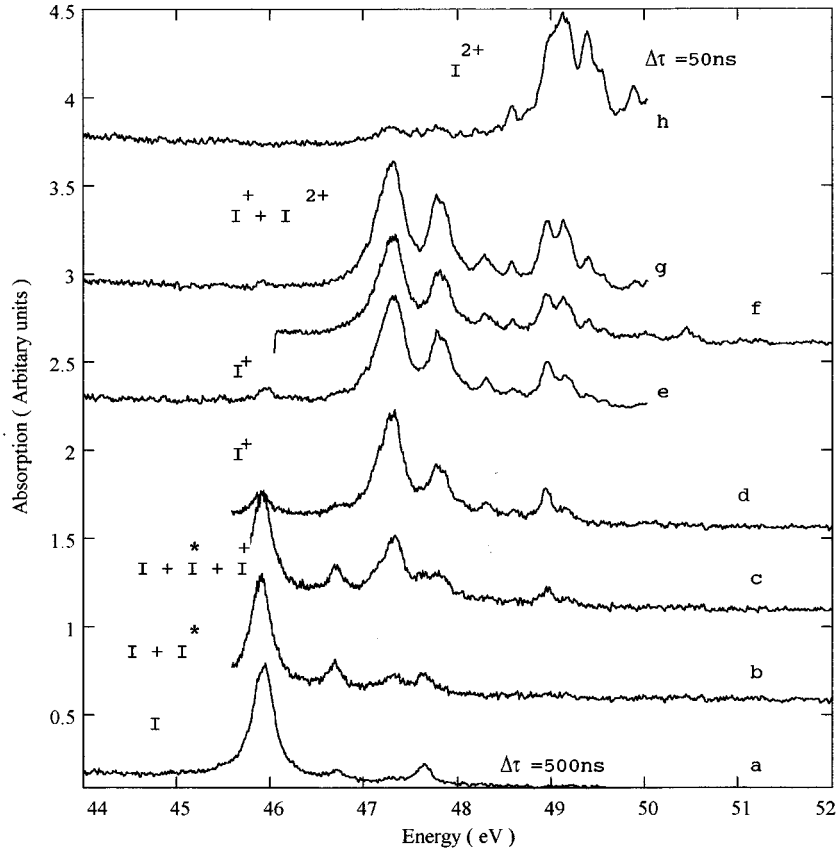

FIG. 1. Structure due to $4d \rightarrow 5p$ photoabsorption in an iodine plasma recorded using the dual laser-produced plasma technique. At the shortest delay, $\Delta\tau = 50$ ns, between the creation of the absorbing and backlighting plasmas the spectrum is almost exclusively due to I^{2+} while at the longest delay, $\Delta\tau = 500$ ns, it is due solely to neutral iodine. At intermediate values of $\Delta\tau$ the contribution due to I^{+} first increases and then decreases as $\Delta\tau$ is increased. (The baseline of each trace has been shifted vertically by an arbitrary amount.)

μm-wide plasma whose length can be varied between 2 and 12 mm. In the present case all data were recorded at a 6-mm plasma column length and a laser pulse power density on target of $\sim 5 \times 10^9$ W cm^{-2}. For photoelectric detection the focal spot has spherical symmetry and a typical diameter of 200 μm. The resulting laser flux is in excess of 10^{10} W cm^{-2}. The backlighting continuum was produced by tightly focusing an 860-mJ, 10-ns, Nd:YAG (yttrium-aluminum-garnet) pulse onto a Sm, Yb, or W target. Variation of the interlaser pulse delay, $\Delta\tau$, displacement of the absorbing plasma from the spectrometer optical axis or irradiance on target makes it possible to obtain spectra in which different ion stages are optimized. After absorption, the transmitted light was dispersed; in the photographic work a 2-m grazing-incidence spectrograph with a reciprocal dispersion which varied from 1.2 Å /mm at 150 Å to 1.6 Å /mm at 300 Å was used while the photoelectric detector consisted of a microchannel plate butt coupled to a phosphor-coated photodiode array placed on the focal curve of a 2.2-m grazing-incidence spectrograph with essentially similar characteristics. Some typical spectra obtained in the 40–60-eV region are presented in Fig. 1; these spectra were recorded photoelectrically and are essentially single-shot spectra. The photographic spectra, in contrast, represent integration over 10^3 laser shots. For $\Delta\tau \leqslant 50$ ns the spectrum was found to contain mainly lines of I^{2+}. For $\Delta\tau \sim 150$ ns it was almost exclusively I^{+} while for $\Delta\tau \geqslant 180$ ns neutral iodine absorption began to contribute. The spectrum of I_2 in this region is well known [13] and it is interesting to note that even at the longest delays investigated ($\Delta\tau = 800$ ns) no absorption due to I_2 was obtained. The spectra were calibrated by superimposing emission lines from an aluminum plasma. For discrete features appearing in both spectra the measurement accuracy is estimated as ± 0.03 eV and is limited by the inherent width of the features.

III. RESULTS

A. $4d \rightarrow 5p$ absorption spectra

1. Neutral iodine

The ground state of neutral iodine is $4d^{10}5s^2 5p^5\ ^2P_{3/2}$ and lines are observed due to $^2P_{3/2} \rightarrow {}^2D_{5/2}$ and $^2P_{3/2} \rightarrow {}^2D_{3/2}$ transitions. In addition the $^2P_{1/2} \rightarrow {}^2D_{3/2}$ line observed by Pettini *et al.* [3] also appears [Figs. 1(a)–1(c) and 2(a)]. Calculations with the Cowan RCN, RCN2, and RCG suite of codes [14] predict the ratio of relative strength of the $^2P_{3/2} \rightarrow {}^2D_{5/2}$ to the $^2P_{3/2} \rightarrow {}^2D_{3/2}$ component to be 9.03, in excellent agreement with the earlier calculation of Nahon *et al.* [6]. The ratio of the theoretical oscillator strengths for $^2P_{1/2} \rightarrow {}^2D_{3/2}$ to $^2P_{5/2} \rightarrow {}^2D_{5/2}$ is 0.55. From the calculated gf values and observed intensities, excited to ground-state

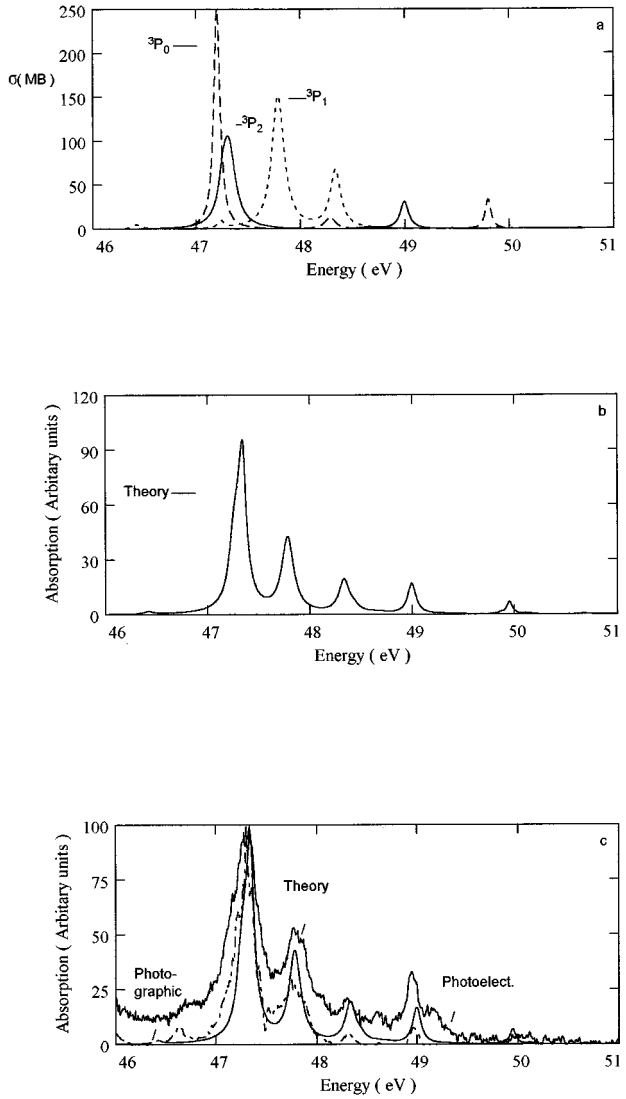

FIG. 2. (a) Theoretical contributions due to the $4d^{10}5s^25p^4{}^3P$ terms to the $4d\rightarrow 5p$ photoabsorption cross section of I^+. (b) The relative contributions of the ^3P terms are weighted as 50:30:20 and summed. (c) Comparison between the theoretical and experimental spectra.

populations ranging from 5% to 30% were inferred for the plasmas responsible for Figs. 1(a)–1(c). These values correspond to electron temperatures T_e of 0.5–2.0 eV, if a Boltzmann distribution between the levels is assumed. In practice the actual value of T_e may be less since at long interplasma delays the collision frequency is reduced because of plasma expansion. In Fig. 1(d) only the $^2P_{3/2}\rightarrow{}^2D_{5/2}$ component is observed and the plasma is dominated by I^+ ions. The energies of the features measured in the present experiment are 45.94 and 47.64 eV for the $^2P_{3/2}\rightarrow{}^2D_{5/2}$ and $^2D_{3/2}$ lines and 46.70 eV for the $^2P_{1/2}\rightarrow{}^2D_{3/2}$ line. These may be compared with previous measured values of 46.2 and 47.9 eV [6] and 45.87 and 47.63 eV [3] for the $^2P_{3/2}\rightarrow{}^2D_{5/2}$, $^2D_{3/2}$ lines and 46.70 eV for the $^2P_{1/2}\rightarrow{}^2D_{3/2}$ line [3].

The experimental linewidths deduced after deconvolution by Nahon *et al.* are 170 meV for the $4d^{-1}5p^2D_{5/2}$ and 155 meV for the $4d^{-1}5p^2D_{3/2}$ [15]. Since the excited ^2D states are known to decay by direct autoionization and in particular the relaxation dynamics of the $^2D_{3/2}$ have been well documented from photoelectron spectra [6], the Cowan HF code was used to calculate the autoionization widths and the branching ratios of the various deexcitation pathways. Nahon *et al.* [6] identified the possible decay processes as

$$4d^95s^25p^6(^2D_{5/2})\rightarrow 4d^{10}5s^25p^4(^3P,{}^1D, \text{ and } {}^1S) + \varepsilon l \quad (l=0,2,4)$$

$$\rightarrow 4d^{10}5s5p^5(^3P \text{and} {}^1P)+\varepsilon l \quad (l=1,3)$$

$$\rightarrow 4d^{10}5s^05p^6(^1S_0)+\varepsilon l \quad (l=2),$$

which they referred to as processes $D1$, $D2$, and $D3$. Their calculations for processes $D1$ and $D3$ were in good agreement with observation. However, for process $D2$, instead of observing four lines in the photoelectron spectrum due to decay to $5s5p^5\,{}^3P_{0,1,2}$ and $^1P_1$ states, they observed ten well-resolved features. They were able to account for these features by the presence of strong configuration mixing of the $5s^25p^35d$ and $5s^25p^36s$ satellite configurations with the $5s5p^5$ and the dominance of decay into the $5s5p^5{}^1P_1$ state. The importance of such satellite configurations to the interpretation of the $4d$ relaxation processes in xenon had already been identified [16–18]. In the present case, the Cowan suite of codes was used to calculate the autoionization widths and branching ratios for decay via the processes $D1$, $D2$, and $D3$. Values of 170 and 155 meV were obtained for the $^2D_{5/2}$ and $^2D_{3/2}$ autoionization widths for a 22% reduction of the F^k, G^k, and R^k parameters. Increasing or decreasing the Slater-Condon parameters by a few percent caused a corresponding increase or decrease in the linewidths and also a change of a few percent in the branching ratios. The results of these calculations are presented in Tables I and II, and are in excellent agreement with experiment. It should be noted that the earlier theoretical results were obtained *ab initio* and

TABLE I. Comparison between theoretical and experimental data for the relative probabilities of the different relaxation mechanisms in the decay of the $4d^95s^25p^6{}^2D_{5/2}$ and $^2D_{3/2}$ states of neutral iodine.

Term (Ref).	Process $D1$	Process $D2$	Process $D3$	Lifetime (fs)	r (meV)
$^2D_{5/2}$ (obs. [6])	0.279	0.648	0.073	24.38	170
(calc. [6])	0.445	0.302	0.025		
(calc. this work)	0.254	0.641	0.105	24.38	170
$^2D_{3/2}$ (obs. [6])				26.90	155
(calc. this work)	0.267	0.622	0.111	26.90	155

that the values we obtain are sensitive to the choice of scaling parameters. For the $^2D_{5/2}$ decay, an attempt was made to introduce configuration interaction effects in process $D2$ by explicit inclusion of the $5s^25p^36s\varepsilon l$ and $5s^25p^35d\varepsilon l$ configurations. However, this failed to reproduce the observed photoelectron spectrum and because of memory constraints it was not possible to increase the final-state basis by introducing further $5s^25p^3nl\varepsilon l'$ configurations. Also Nahon *et al.* [6] noted from their experimental data that for process $D2$, decay to the $4d^{10}5s5p^5{}^1P_1$ rather than the ^3P is preferred, with the $^1P_1$ relaxation being 3.61 times more probable. Our calculations give ratios of 3.67 for the $^2D_{5/2}$ decay and 6.35 for the $^2D_{3/2}$.

2. Singly ionized iodine

For I^+, the ground state is $4d^{10}5s^25p^4\,{}^3P_2$ and the $^3P_{0,1}$, $^1D_2$, and $^1S_0$ levels were previously found to lie 0.86, 1.72, and 3.70 eV higher in energy [19]. Calculations were performed for $4d$ excitation using an excited-state basis containing $4d^95s^25p^4(np+mf)$ states with $5\leqslant n\leqslant 10$, $4\leqslant m\leqslant 12$ and discretized continuum states of the form $4d^95s^25p^4\varepsilon p,\varepsilon f$ for a range of energies up to 4 Ry above the $4d^{-1}$ threshold [14]. For these calculations the Slater-Condon parameters were again reduced by 22% since this scaling gave best agreement between theory and experiment in neutral iodine for energies, linewidths, and relaxation amplitudes. This scaling, which is typical for $4d$ excitation [20], was used throughout this work and was seen to give good agreement for energy positions in the ions; in each case the largest discrepancies between observed and calculated energies could be traced to the configuration average energy $E_{\rm av}$ and were not as greatly influenced by other choices of scaling factor for F^k, G^k, and R^k parameters as the rate-dependent quantities. The energies and eigenvector compositions deduced from the calculation for the $4d^95s^25p^5$ terms are presented in Table III, while theoretical transition energies and gf values are listed in Table IV. The coupling scheme is seen to be best described by $(d^9(j_1),p^5(j_2))_j$ rather than LSJ although the latter scheme is retained for simplicity of notation. It is interesting to note the evolution of the I^+ spectrum in Fig. 1. In Fig. 1(b) a weak feature appears at 47.32 eV which corresponds to the strongest transition from the ground level, i.e., $^3P_2\rightarrow{}^3D_3$, and indicates an I^+/I ratio of $<5\%$. In Fig. 1(c) the relative population has increased to $\sim 30\%$ and lines due to photoabsorption from the $^3P_2$, $^3P_0$, and $^3P_1$ states are present. In Figs. 1(d) and 1(e), the I^+ population exceeds 95% and the spectrum can still be completely described by considering only absorption from the ^3P levels. In Figs. 1(f) and 1(g) some additional features due to I^+ absorption appear at higher energies and there is some evidence for a ''shoulder'' at 47.86 eV merged with $^3P_1\rightarrow{}^3D_2$ line. This shoulder, if real, could represent a contribution from the strong $^1D_2$-$^1F_3$ line predicted to lie at 47.659 eV ($gf=1.154$). A weaker shoulder at 47 eV may arise from the $^1D_2$-$^3F_3$ line predicted to lie at 46.903 eV. However, further $^1D_2$-based transitions, in particular $^1D_2$-$^1D_2$ predicted to lie at 45.451 eV, was absent. From Table IV it is seen that the calculated and observed transition energies generally agree to within 0.1 eV, while the gf values correlate very well with the observed intensities. Also, it should be noted that it was possible to deduce a value of 0.84 eV for the $4d^{10}5s^25p^4\,{}^3P_1$ energy which agrees with the value of Ref. [19] to within experimental error.

Relaxation of the $4d^95s^25p^5$ states is assumed to be by direct autoionization; the decay processes will then be

$$\begin{aligned} 4d^95s^25p^5(^{1,3}P,^{1,3}D,^{1,3}F)&\rightarrow 4d^{10}5s^25p^3(^4S,^2P,^2D)+\varepsilon l(l=0,2,4)\quad(\text{process } D1)\\ &\rightarrow 4d^{10}5s5p^4(^2S,^{2,4}P,^2D)+\varepsilon l(l=1,3)\quad(\text{process } D2)\\ &\rightarrow 4d^{10}5p^5(^2P)+\varepsilon l(l=2)\quad(\text{process } D3). \end{aligned}$$

Calculations were performed to extract linewidths and branching ratios with the usual scaling of parameters. Because of the excellent agreement achieved with the experimental data for neutral iodine, similar scalings were chosen throughout for I^+ and I^{2+}. The observed linewidths in Table IV are taken from both the photographic and photoelectronic data. For the former, the strongest features are likely to be overestimated while the weaker lines are underestimated because of plate-saturation effects; for the latter poor signal-to-noise ratio for the weak features and line overlapping for the strongest transitions in some cases limit the resolution. The observed linewidths were obtained by direct comparison with the neutral iodine features whose widths are known very accurately. The estimated accuracy of the values quoted in Table IV is ± 50 meV, and in every case they agree with the calculated values to within experimental error. The average probabilities associated with the different decay processes were calculated to be 0.288, 0.590, and 0.122 for pathways $D1$, $D2$, and $D3$. The detailed term-by-term values are listed in Table V. Note that process $D3$ was not permitted for the $4d^95s^25p^5{}^3P_1$, $^3D_3$, and $^1D_2$ states as the double $5s$ hole state is calculated to be higher in energy. In performing these calculations the term energy of the $4d$ hole state was first obtained and the kinetic energy with respect to the configuration average energies of the final states then calculated. These values were used for the continuum εl electrons. In neutral iodine it was noted that the choice of the final-state term energy rather than the configuration average energy $E_{\rm av}$ did not affect the calculation significantly, and the situation in I^+ was found to be similar.

Finally, in Fig. 2(a) direct comparison is made between theory and experiment. In constructing the theoretical spectrum for I^+ the calculated energies, linewidths, and gf values were used and the individual contributions due to each of

TABLE II. Comparison between theoretical and experimental results for the relative populations in the $4d^{10}5s^25p^4$ configuration produced by $4d^95s^25p^6\ ^2D_{5/2}$ and $^2D_{3/2}$ relaxation.

State	$^2D_{5/2}$ (obs. [6])	$^2D_{5/2}$ (calc.[6])	$^2D_{5/2}$ (calc. this work)	$^2D_{3/2}$ (calc. this work)
$^3P_2$	0.247	0.225	0.285	0.065
$^3P_1$	0.188		0.089	0.130
$^3P_0$			0.119	0.001
$^1D_2$	0.345	0.489	0.319	0.471
$^1S_0$	0.227	0.286	0.188	0.333

the ^3P sublevels evaluated separately using the fact that the cross section σ can be written [14] as

$$\sigma=\frac{\pi\hbar e^2}{2m\varepsilon_0 c}f_k/2\pi[(E_k-E)^2+\Gamma_k^2/4],$$

where E_k and Γ_k are the energy and linewidth of the transition and f_k is the oscillator strength. The individual contributions are shown in Fig. 2(a) and when summed in the ratio $^3P_2/^3P_1/^3P_0=50{:}30{:}20$ give a good fit to the particular set of experimental data used. It should be noted that this ratio corresponds to an equilibrium distribution for $T_e>2$ eV at which the $^1D_2$ contribution should be 40% of the $^3P_2$, yet discrete $^1D_2$ lines are not observed, though, as mentioned before, there is some evidence for $^1P_2$-$^1F_3$ and $^3F_3$ transitions merged with the stronger features.

3. Doubly ionized iodine

In Fig. 1(g) the spectrum obtained for an interlaser delay τ of 130 ns is presented. In addition to the I^+ lines of Fig. 1(f) additional features are weakly evident at higher energies. At the higher plasma temperatures achieved at shorter delays some additional I^+ lines due to $^1D_2$ or $^1S_0$ excitation might be expected. Since these lines predominantly occur on the low-energy side of the ^3P excitation spectrum and as no lines are observed there, additional excited-state absorption from I^+ cannot be responsible and the additional features are due to transitions in I^{2+}. Indeed, for $\Delta\tau<100$ ns the spectrum is almost exclusively due to I^{2+}, which gives rise to a composite feature with two distinct peaks extending from approximately 49 to 50 eV, with some additional weak features extending some 1 eV on either side. The ground state of this ion is $4d^{10}5s^25p^3\,^4S_{3/2}$ while the $^2D_{3/2}$, $^2D_{5/2}$, $^2P_{1/2}$, and $^2P_{3/2}$ levels are predicted to be 1.77, 2.137, 3.432, and 3.991 eV higher in energy. Calculations were again performed for this spectrum and the results summarized in Tables VI and VII. As before, the spectrum may be almost completely explained by limiting consideration to the ground and lower (^2D) levels. The excited-state lifetimes were calculated and the average relaxation probabilities to $4d^{10}5s^25p^2\varepsilon l$ and $4d^{10}5s5p^3\varepsilon$ states were found to be 0.342 and 0.658, respectively. Direct autoionization to the

TABLE III. Energies and eigenvector compositions of the $4d^{10}5s^25p^4$ and $4d^95s^25p^5$ configurations of I^+.

Configuration	Term	E_{Cowan} (eV)	$E_{\text{obs.}}$ (eV)	J	%LS	%jj
$4d^{10}5s^25p^4$	^3P	0.0	0.0	2	91% ^3P+9% ^1D	
	^3P	0.828	0.86	0	88% ^3P−12% ^1S	
	^3P	0.831	0.84	1	100% ^3P	
	^1D	1.698	1.72	2	91% ^1D−9% ^3P	
	^1S	3.530	3.70	0	88% ^1S+12% ^3P	
$4d^95s^25p^5$	^1D	47.149	47.15	2	67% ^1D−17% ^3P−12% ^3D	92% (5/2,1/2)+7% (5/2,3/2)
	^3D	47.206	47.32	3	89% ^3D+10% ^1F	94% (5/2,1/2)
	^3P	47.961	48.07	1	46% ^1P+28% ^3P−25% ^3D	95% (5/2,1/2)
	^3D	48.507		2	−78% ^3D+20% ^3P	59% (5/2,3/2)+38% (3/2,1/2)
	^3F	48.601		3	83% ^3F+12% ^1F−5% ^3D	82% (5/2,3/2)+16% (3/2,3/2)
	^3P	48.890	48.95	2	61% ^3P−18% ^1D+13% ^3F+9% ^3D	60% (3/2,1/2)−34% (5/2,3/2)
	^3D	49.060	49.17	1	55% ^3D+45% ^3P	91% (3/1,1/2)+7% (3/2,3/2)
	^1F	49.357		3	78% ^1F−15% ^3F−6% ^3D	−83% (3/2,3/2)+14% (5/2,3/2)
	^3P	49.437		0	100% ^3P	100% (3/2,3/2)
	^3F	50.025		2	−81% ^3F−14% ^1D	99% (3/3,3/2)
	^1P	50.572		1	54% ^1P−26% ^3P+20% ^3P+20% ^3D	90% (3/2,3/2)−8% (3/2,1/2)

TABLE IV. Theoretical and experimental energies and linewidths, calculated gf values and relative intensities of the most intense $4d^{10}5s^25p^4-4d^95s^25p^5$ transitions observed in the spectrum of I^+.

Transition	E_{HF} (eV)	gf	Γ_{HF} (eV)	$E_{obs.}$ (eV)	I	$\Gamma_{obs.}$ (eV)
$^3P_0$-$^3P_1$	47.133	0.529	0.072	47.15	40	0.105
$^3P_1$-$^1D_2$	47.149	0.218	0.098			
$^3P_2$-$^3D_3$	47.206	1.005	0.152	47.32	100	0.150
$^3P_1$-$^3D_2$	47.676	0.614	0.141	47.80	60	0.150
$^3P_2$-$^3P_1$	47.961	0.030	0.072	48.07	5	
$^3P_1$-$^3D_1$	48.229	0.226	0.121	48.32	20	0.105
$^3P_0$-$^3D_1$	48.232	0.042	0.121			
$^3P_2$-$^3D_2$	48.507	0.012	0.141	48.63	10	0.150
$^3P_1$-$^3P_0$	48.606	0.080	0.089			
$^3P_2$-$^3P_2$	48.890	0.220	0.098	48.95	30	0.095
$^3P_2$-$^3D_1$	49.060	0.084	0.121	49.17	20	0.105

$4d^{10}5p^4$ configuration is not possible as it is higher in energy than the $4d^95s^25p^3$. The detailed term-by-term values are listed in Table VIII. It should be noted that in each case the partial linewidth due to autoionization exceeds that due to radiative decay by between three and four orders of magnitude and so essentially determines the experimentally observed values (Table VII). No attempt was made to extract experimental linewidths because of the blended nature of the lines observed. As before, in Fig. 3 direct comparison is made between theoretical and experimental results. The individual contributions of the different levels of the ground configuration were first evaluated and summed in a ratio $^4S_{3/2}$:$^2D_{3/2}$:$^2D_{5/2}$:$^2P_{3/2}$:$^2P_{1/2}$ of 45:35:12:5:3, which corresponds to a thermal distribution with $T_e\sim 2$ eV. This combination reproduces the experimental spectrum recorded photoelectrically quite well. The photographic spectrum is dominated by two peaks at 49.08 and 49.16 eV which arise primarily from $^4S_{3/2}\rightarrow{}^2P_{3/2}$ and $^4P_{5/2}$ transitions mixed in with I^+ features. There is only a very minor contribution from excited-state (^2D) absorption, which points to a much lower average electron temperature in this case. Since the collision frequency is much greater at short interplasma delays where higher densities in the absorbing plasma prevail it is expected that equilibrium excited-state populations would be most likely observed in higher ion stages.

To gain some insight into the plasma conditions, it is of interest to use the steady-state collisional-radiative model of Colombant and Tonon [21] to calculate the relative populations of different ion stages as a function of n_e and T_e. T_e was first estimated for the laser fluxes used in the experiment, n_e was set at the cutoff density of ruby laser light (2.4×10^{21} cm^{-3}), and the evolution of fractional number density as a function of T_e was computed. The results of these calculations are presented in Fig. 4(a); values of T_e corresponding to the laser fluxes used are indicated in this figure. It is seen that the initial ion populations at the target surface at $\Delta\tau=0$ in the photoelectric and photographic experiments are quite different. In the former, the predicted population is 18% I^{4+} + 39% I^{3+} + 37% I^{2+} + 4% I^+ while

TABLE VII. Theoretical and experimental energies, calculated linewidths, and gf values and relative intensities of the most intense $4d^{10}5s^25p^3$-$4d^95s^25p^4$ transitions observed in the spectrum of I^+.

TABLE V. Theoretical relative decay probabilities, lifetimes, and autoionizing linewidths of the $4d^95s^25p^5\ ^{2s+1}L_J$ levels of I^+.

J	Term	Process $D1$	Process $D2$	Process $D3$	Lifetime (fs)	Γ (eV)
0	^3P	0.243	0.568	0.189	46.3	0.089
1	^3P	0.370	0.630		57.7	0.072
	^3D	0.331	0.528	0.141	34.1	0.121
	^1P	0.311	0.443	0.246	62.2	0.067
2	^3P	0.230	0.596	0.174	42.1	0.098
	^3D	0.348	0.525	0.128	29.3	0.141
	^3F	0.134	0.675	0.191	47.6	0.087
	^1D	0.252	0.749		21.2	0.098
3	^3D	0.395	0.605		27.1	0.152
	^3D	0.164	0.678	0.158	37.2	0.111
	^1F	0.390	0.494	0.116	28.4	0.146

TABLE VI. Calculated energies and eigenvector compositions of the $4d^{10}5s^25p^3$ and $4d^95s^25p^4$ configurations of I^{2+}.

Configuration	J	Term	E_{Cowan} (eV)	%LS	%jj
$4d^{10}5s^25p^3$	1/2	^2P	3.205	100% ^2P	
	3/2	^4S	0.0	91% ^4S+8% ^2P	
		^2D	1.529	80% ^2D−15% ^2P	
		^2P	3.639	77% ^2P+19% ^2D	
	5/2	^2D	1.910	100% ^2D	
$4d^95s^25p^4$	1/2	$(^3P)^2P$	48.595	78% $(^3P)^2P$+8% $(^3P)^4P$−6% $(^3P)^4D$	92% $(5/2,^3P_2)$+7% $(5/2,^1D_2)$
		$(^3P)^4P$	50.327	84% $(^3P)^4P$	92% $(3/2,^3P_2)$
		$(^3P)^4D$	51.724	66% $(^3P)^4D$+16% $(^1D)^2S$−15% $(^1D)^2P$	77% $(3/2,^3P)$+20% $(5/2,^1D_2)$
		$(^1D)^2P$	51.780	30% $(^1D)^2S$−30% $(^1D)^2P$−21% $(^3P)^4D$−16% $(^3P)^2P$	70% $(5/2,^1D)$−24% $(3/2,^3P_1)$
		$(^1D)^2S$	53.297	49% $(^1D)^2S$+45% $(^1D)^2P$	92% $(3/2,^1D_2)$
	3/2	$(^3P)^2P$	48.929	46% $(^3P)^2P$+38% $(^3P)^4P$+9% $(^3P)^2D$	84% $(5/2,^3P_2)$−9% $(5/2,^3P_1)$
		$(^3P)^4P$	50.296	27% $(^3P)^4F$−26% $(^3P)^2D$+17% $(^3P)^4P$+16% $(^1D)^2D$	−54% $(5/2,^3P_1)$−14% $(5/2,^1D_2)$+11% $(3/2,^3P_2)$+9% $(3/2,^3P_0)$
		$(^3P)^4D$	50.392	39% $(^3P)^4D$+27% $(^3P)^4P$−22% $(^3P)^2P$+6% $(^1D)^2P$	67% $(3/2,^3P_2)$+18% $(5/2,^3P_1)$+8% $(3/2,^1D_2)$
		$(^1D)^2D$	51.126	38% $(^1D)^2P$−33% $(^1D)^2D$−10% $(^3P)^4D$−7% $(^3P)^2P$ −6% $(^3P)^2D$	69% $(5/2,^1D_2)$+9% $(3/2,^3P_0)$−9% $(5/2,^3P_1)$−7% $(5/2,^3P_2)$
		$(^3P)^4F$	51.394	55% $(^3P)^4F$+17% $(^3P)^4D$+10% $(^3P)^2P$−10% $(^3P)^4P$	88% $(3/2,^3P_1)$
		$(^3P)^2D$	51.868	50% $(^3P)^2D$−21% $(^3P)^4D$−14% $(^1S)^2D$−8% $(^3P)^2P$	56% $(3/2,^3P_0)$−14% $(3/2,^1S_0)$−11% $(3/2,^3P_2)$+7% $(5/2,^3P_1)$
		$(^1D)^2P$	52.649	47% $(^1D)^2P$+37% $(^1D)^2D$−6% $(^3P)^4P$	79% $(3/2,^1D_2)$−9% $(3/2,^3P_2)$+6% $(5/2,^1D_2)$
		$(^1D)^2D$	54.872	80% $(^1S)^2D$	80% $(3/2,^1S_0)$+14% $(3/2,^3P_0)$
	5/2	$(^3P)^4P$	49.078	63% $(^3P)^4P$+12% $(^1D)^2D$+9% $(^3P)^2F$	63% $(5/2,^3P_2)$+13% $(5/2,^1D_2)$+9% $(5/2,^3P_0)$−8% $(5/2,^3P_1)$
		$(^3P)^4F$	49.842	44% $(^3P)^4F$+20% $(^3P)^2F$−14% $(^1S)^2D$ −10% $(^3P)^2D$−7% $(^3P)^4D$	51% $(5/2,^3P_2)$+20% $(5/2,^3P_1)$−14% $(5/2,^3P_1)$−14% $(5/2,^1S_0)$ −6% $(5/2,^3P_2)$
		$(^3P)^4D$	49.994	48% $(^3P)^4D$+20% $(^3P)^2F$−19% $(^3P)^1P$+8% $(^3P)^2D$	66% $(5/2,^3P_1)$+16% $(5/2,^3P_2)$−12% $(5/2,^3P_0)$
		$(^1D)^2D$	50.495	52% $(^1D)^2D$−30% $(^1D)^2F$−12% $(^3P)^4P$	79% $(5/2,^1D_2)$−7% $(5/2,^3P_2)$
		$(^3P)^2F$	50.844	40% $(^3P)^2F$−22% $(^3P)^4D$−17% $(^3P)^4D$+11% $(^3P)^4D$	−70% $(3/2,^3P_2)$−7% $(3/2,^3D_2)$−7% $(3/2,^3P_1)$+6% $(5/2,^3P_0)$
		$(^1D)^2F$	51.642	34% $(^3P)^4F$−29% $(^1D)^2F$+19% $(^3P)^2D$−10% $(^1D)^2D$	55% $(3/2,^3P_1)$−38% $(3/2,^1D_2)$
		$(^3P)^2D$	52.540	36% $(^3P)^2D$+33% $(^1D)^2F$+12% $(^1D)^2D$−10% $(^3P)^4D$	45% $(3/2,^1D_2)$+32% $(3/2,^3P_1)$−19% $(3/2,^3P_2)$
		$(^1S)^2D$	53.398	74% $(^1S)^2D$+7% $(^1D)^2D$−6% $(^3P)^2D$	75% $(5/2,^1S_0)$+16% $(5/2,^1P_0)$
	7/2	$(^1D)^2P$	48.927	24% $(^1D)^2F$+31% $(^3P)^4D$+27% $(^3P)^2F$+17% $(^3P)^4F$	71% $(5/2,^3P_2)$+25% $(5/2,^1D_2)$
		$(^3P)^4F$	49.970	68% $(^3P)^4F$−30% $(^3P)^4D$	83% $(5/2,^3P_1)$+12% $(5/2,^3P_2)$
		$(^3P)^4D$	50.577	39% $(^3P)^4D$−30% $(^1D)^2F$−13% $(^3P)^2F$+11% $(^3P)^4F$	39% $(3/2,^3P_2)$−37% $(5/2,^1D_2)$+15% $(5/2,^3P_2)$
		$(^3P)^2F$	51.092	55% $(^3P)^4F$−42% $(^1D)^2F$	−40% $(3/2,^3P_2)$−35% $(5/2,^1D_2)$+11% $(5/2,^3P_2)$
		$(^1D)^2G$	52.775	89% $(^1D)^2G$	90% $(3/2,^1D_2)$−9% $(3/2,^3P_2)$

TABLE VII. Theoretical and experimental energies, calculated linewidths, and *gf* values and relative intensities (based on peak heights) of the most intense $4d^{10}5s^25p^3$-$4d^95s^25p^4$ transitions observed in the spectrum of I^+.

Transition	E_{Cowan} (eV)	gf	Γ_{HF} (meV)	E_{obs} (eV)	I
$^2P_{1/2}$-(^3P)$^2P_{1/2}$	45.576	0.022	42		
$^2P_{3/2}$-(^1D)$^2D_{5/2}$	46.856	0.028	76		
$^2P_{1/2}$-(^3P)$^4D_{3/2}$	47.358	0.045	46		
$^2D_{3/2}$-(^3P)$^2P_{3/2}$	47.400	0.050	42	47.50	10
$^2D_{3/2}$-(^3P)$^4P_{5/2}$	47.548	0.079	102		
$^2P_{3/2}$-(^3P)$^4F_{3/2}$	47.755	0.039	47		
$^2D_{3/2}$-(^3P)$^4F_{3/2}$	47.933	0.021	59		
-(^3P)$^4D_{5/2}$	48.084	0.033	55		
$^2P_{1/2}$-(^1D)$^2D_{3/2}$	48.094	0.143	39		
$^2D_{3/2}$-(^3P)$^4F_{5/2}$	48.313	0.109	59	48.40	10
-(^3P)$^4D_{5/2}$	48.464	0.195	55		
$^2D_{5/2}$-(^1D)$^2D_{5/2}$	48.585	0.153	76	48.60	25
$^4S_{3/2}$-(^3P)$^2P_{1/2}$	48.604	0.046	42		
$^2P_{1/2}$-$^1D^2S_{1/2}$	48.747	0.168	20		
$^2D_{3/2}$-(^3P)$^4P_{3/2}$	48.766	0.247	65		
-(^3P)$^4P_{1/2}$	48.790	0.029	88		
$^2P_{3/2}$-(^3P)$^2D_{5/2}$	48.811	0.667	57		
$^2P_{3/2}$-(^2P)$^2D_{3/2}$	48.830	0.484	53		
$^4S_{3/2}$-(^3P)$^2P_{3/2}$	48.929	0.369	62	49.08	50
$^2D_{5/2}$-(^3P)$^2F_{5/2}$	48.934	0.239	73		
$^2D_{3/2}$-(^1D)$^2D_{5/2}$	48.965	0.390	76		
$^2P_{3/2}$-(^1D)$^2P_{3/2}$	49.011	0.353	37		
$^4S_{3/2}$-(^3P)$^4P_{5/2}$	49.078	0.823	102	49.16	100
$^2D_{5/2}$-(^3P)$^2F_{7/2}$	49.182	1.979	55		
$^2D_{5/2}$-(^1D)$_{3/2}$	49.216	0.037	39	49.44	70
$^2D_{3/2}$-(^3P)$^2F_{5/2}$	49.314	0.412	73		
-(^1D)$^2D_{3/2}$	49.596	0.066	39	49.89	10
$^2P_{3/2}$-(^1D)$^2S_{1/2}$	49.656	0.184	20		
$^2D_{5/2}$-(^1D)$^2F_{5/2}$	49.737	0.220	49		
$^2P_{3/2}$-(^1S)$^2D_{5/2}$	49.759	0.487	59		
$^2D_{3/2}$-(^3P)$^4F_{3/2}$	49.864	0.083	47	49.95	20
$^4S_{3/2}$-(^3P)$^4D_{5/2}$	49.994	0.103	55		
$^2D_{3/2}$-(^1D)$^2F_{5/2}$	50.117	0.023	49		
$^4S_{3/2}$-(^3P)$^4P_{3/2}$	50.296	0.053	65		
-(^3P)$^4P_{1/2}$	50.319	0.247	88	50.51	50
$^2D_{3/2}$-(^3P)$^2D_{3/2}$	50.339	0.049	53		
$^4S_{3/2}$-(^3P)$^4D_{3/2}$	50.392	0.152	46		
-(^1D)$^2D_{3/2}$	50.495	0.028	76		
$^2D_{5/2}$-(^1D)$^2D_{3/2}$	50.739	0.140	37		
$^2D_{3/2}$-(^3P)$^2D_{5/2}$	50.920	0.082	57		
$^4S_{3/2}$-(^3P)$^4F_{3/2}$	51.394	0.025	47		
$^2D_{5/2}$-(^1S)$^2D_{5/2}$	51.488	0.058	59		
$^2D_{1/2}$-(^1S)$^2D_{3/2}$	51.820	0.049	30		

in the latter it is predicted as 8% I^{2+} + 57% I^+ + 33% I. To observe I^+ at maximum concentration requires $T_e = 4.0$ eV while I^{2+} requires 5.5 eV, both of which are considerably greater than the values deduced from excited-state distributions. Furthermore, the fact that I^{2+} absorption was obtained in the photographic spectra at delays > 50 ns indicates that the ion ratios of Fig. 4 should be biased in favor of higher ζ constituents. If, however, one assumes a lower average n_e, which is definitely the case away from the target surface and after the plasma priming pulse has ceased, then for a given T_e, the average ζ is higher because of the decrease in the three-body recombination rate [Fig. 4(b)]. In the collisional-radiative plasma regime collisional ionization is balanced by three-body recombination and radiative decay and the latter becomes the dominant deexcitation mechanism for $n_e < 10^{19}$ cm^{-3} as the equilibrium tends towards coronal.

B. $4d \rightarrow 6p$ transitions

The $4d \rightarrow np$, $n > 5$ spectrum was found by Nahon and Morin [7] to consist of a group of resonances in the 55–59-eV spectral region, about half of which lie above the $4d^2D_{5/2}$ threshold at 57.42 eV. They made no attempt at detailed assignments but found a similar proximity of the first $3d^95p$ resonance in bromine to the $3d^{92}D_{5/2}$ limit. This situation contrasts with the rare gases where the first level is well below threshold and a well-developed Ryberg series is observed. In the present case features were again obtained in the spectrum of neutral iodine and are presented in Fig. 5. The earlier data displayed five well-resolved peaks with evidence of further substructure when recorded at a photon band pass of 0.13 eV. In the present case a systematic shift of approximately 0.4 eV towards lower energy is observed. Moreover, the fourth peak resolves into two further features while an additional weak resonance was noted at 55.87 eV and some others were obtained at higher energy. In order to identify these lines calculations were performed for $4d \rightarrow np$ transitions using $4d^95s^2[5p^6 + 5p^5(6p + 7p + 8p + 9p + 10p + 4f)]$ as an excited-state basis. From these calculations it was possible to make the assignments listed in Table IX. Although the calculations predict well in excess of 400 lines extending from 54.2 past 60 eV, consideration of only the strongest transitions, those with $gf > 10^{-3}$ involving $^2P_{3/2}$ excitation only successfully reproduce the strongest observed lines. In each case all of these features are seen to consist of blends of more than one transition while the pre-

TABLE VIII. Theoretical relative decay probabilities, lifetimes, and autoionizing linewidths of the $4d^9 5s^2 5p^5\ ^{2s+1}L_J$ levels of I^{2+}.

J	Term	Process $D1$	Process $D2$	Lifetime (fs)	Γ (eV)
1/2	$(^3P)^2P$	0.239	0.761	98	0.042
	$(^3P)^4P$	0.479	0.521	47	0.088
	$(^3P)^4D$	0.399	0.601	222	0.019
	$(^1D)^2P$	0.058	0.942	134	0.031
	$(^1D)^2S$	0.446	0.554	207	0.020
3/2	$(^3P)^2P$	0.396	0.604	66	0.062
	$(^3P)^4P$	0.349	0.551	64	0.065
	$(^3P)^4D$	0.266	0.735	90	0.046
	$(^1D)^2D$	0.347	0.653	106	0.039
	$(^3P)^4F$	0.229	0.771	187	0.047
	$(^3P)^2D$	0.466	0.534	78	0.053
	$(^1D)^2P$	0.413	0.587	112	0.037
	$(^1S)^2D$	0.457	0.543	139	0.030
5/2	$(^3P)^4P$	0.474	0.526	41	0.102
	$(^3P)^4F$	0.224	0.776	70	0.059
	$(^3P)^4D$	0.290	0.710	75	0.055
	$(^1D)^2D$	0.439	0.561	54	0.076
	$(^3P)^2F$	0.418	0.582	57	0.073
	$(^1D)^2F$	0.295	0.705	85	0.049
	$(^3P)^2D$	0.552	0.448	72	0.057
	$(^1S)^2D$	0.515	0.485	74	0.059
7/2	$(^1D)^2F$	0.112	0.888	71	0.058
	$(^3P)^4F$	0.112	0.888	74	0.055
	$(^3P)^4D$	0.141	0.859	88	0.047
	$(^3P)^2F$	0.585	0.414	33	0.133
	$(^1D)^2G$	0.183	0.817	115	0.041

dicted energy is approximately 0.15 eV too low. The weak previously unreported feature noted at 55.87 eV was found to arise from $^2P_{1/2}$ excitation. The assignments for the additional weak structures past 57.75 eV are somewhat tentative since the predicted gf values are very sensitive to the choice of basis. Inclusion of extra p or f states leads to some redistribution of oscillator strength between different transitions in this region.

Combet-Farnoux [22] has addressed the decay mechanism of excited $4d^9 5s^2 5p^5 np$ states and concluded that direct autoionization in which the $6p$ electron acts as a spectator or is involved in a shakeup process is the most important route for decay to the $4d^{10} 5s^2 5p^3 6p$, while second-step autoionization is only weakly possible. Decay to the $4d^{10} 5s 5p^4 6p$ can be followed by further autoionization in which the $6p$ electron can participate. As n increases the production of doubly charged ions becomes more probable by two-electron shakeoff in which both the Rydberg and a $5p$ electron are simultaneously ejected. It should be noted, however, that in analogous $3d$ excitation spectra the $3d^9 nl$ linewidths remained essentially constant [23] with increasing n, which contrasts with the theoretical predictions of Fano and Cooper [24]. Hayashi *et al.* [25] have attributed this to the increased importance of shakeoff with increasing n, which essentially compensates for the decrease in the direct autoionization rate. No attempt was made to calculate linewidths, but a synthetic spectrum in which each transition was assigned an artificial width of 0.1 eV was constructed. An excited-state $^2P_{1/2}$ population of 20% was also assumed. The comparison between the spectrum and the experimental data is presented in Fig. 5.

From the I^+ and I^{2+} calculations, the approximate energies of the strongest $4d \rightarrow 6p$ features in these ions were deduced. Only two broad features centered at 60.77 and 61.21 eV have an intensity comparable to that of the neutral lines, since the $4d \rightarrow 6p$ multiplet is more complex and the available oscillator strength is divided across a larger number of lines. As a consequence, no further $4d \rightarrow 6p$ transitions could be identified in the spectrum of I^+ or I^{2+}.

C. $4d \rightarrow \varepsilon f$ transitions

1. Neutral iodine

Without doubt, the most striking feature in the $4d$ photoabsorption spectrum of iodine in the present series of experiments is the $4d \rightarrow \varepsilon f$ shape resonance. As already indicated, no discrete $4d \rightarrow nf$ transitions are observed since the nf wave functions are eigenstates of the outer well of the bimo-

TABLE IX. Predicted and observed energies of the most intense[a] $4d \rightarrow np$ transitions in the spectra of neutral and singly ionized iodine.

Ion	Transition	E_{HF} (eV)	gf	E_{obs} (eV)	I
I	$^2P_{3/2} \rightarrow 6p(^1D)^2P_{3/2}$	55.199	0.002	55.36–55.52	10
	$6p(^1D)^2P_{1/2}$	55.222	0.003		
	$6p(^3P)^2P_{3/2}$	55.263	0.002		
	$6p(^3D)^2D_{5/2}$	55.300	0.007		
	$6p(^3F)^2D_{5/2}$	55.438	0.017		
	$^2P_{1/2} \rightarrow 6p(^3D)^2P_{1/2}$	55.639	0.004	55.87	2
	$6p(^3D)^2D_{1/2}$	55.677	0.002		
	$6p(^3F)^4D_{3/2}$	55.741	0.010		
	$^2P_{3/2} \rightarrow 6p(^1P)^2S_{1/2}$	55.971	0.002	56.16	3
	$6p(^1P)^2P_{1/2}$	56.016	0.002		
	$6p(^1P)^2P_{3/2}$	56.035	0.001		
	$^2P_{3/2} \rightarrow 7p(^1D)^2P_{3/2}$	56.414	0.001	56.73	4
	$6p(^3D)^4P_{3/2}$	56.500	0.005		
	$6p(^1F)^2D_{3/2}$	56.222	0.001		
	$^2P_{3/2} \rightarrow 6p(^3F)^4D_{5/2}$	56.654	0.004		
	$6p(^3F)^4F_{3/2}$	56.681	0.003		
	$^2P_{3/2} \rightarrow 6p(^3P)^2D_{5/2}$	56.924	0.002	57.05	4
	$8p(^3D)^2P_{3/2}$	56.929	0.001		
	$^2P_{3/2} \rightarrow 6p(^3P)^4D_{3/2}$	57.058	0.003	57.26	4
	$8p(^3F)^2D_{5/2}$	57.064	0.004		
	$6p(^3D)^2F_{5/2}$	57.106	0.001		
	$^2P_{3/2} \rightarrow 9p(^3F)^2D_{5/2}$	57.291	0.005	57.61	4
	$\rightarrow 6p(^1F)^2D_{5/2}$	57.404	0.008		
	$\rightarrow 6p(^3P)^4D_{1/2}$	57.457	0.002		
	$^2P_{3/2} \rightarrow 7p(^3D)^4D_{3/2}$	57.750	0.001	57.93	2
	$^2P_{3/2} \rightarrow 7p(^3D)^4D_{1/2}$	58.306	0.001	58.45	1
	$^2P_{3/2} \rightarrow 8p(^3P)_{5/2}$[b]	58.650	0.001	58.80	1
	$8p(^3P)^2D_{5/2}$[b]	58.668	0.001		
I^+	$^2P_2 \rightarrow 6p(^3P)^3P_2$	60.898	0.010	60.66–60.88	4
	$6p(^3P)^5P_3$	60.951	0.009		
	$6p(^3P)^3D_3$	60.996	0.030		
	$\rightarrow 6p(^3P)^5S_2$	61.189	0.010	61.02–61.32	4
	$6p(^3P)^5P_2$	61.239	0.008		
	$6p(^3P)^5P_3$	61.249	0.007		
	$6p(^3P)^1P_1$	61.272	0.017		
	$6p(^3P)^5D_3$	61.280	0.024		
	$6p(^3P)^3P_2$	61.379	0.025		

[a]For neutral iodine only transitions with $gf > 0.001$ are listed, while for I^+ only those with $gf > 0.005$ are included.

[b]Leading eigenvector quoted in each case.

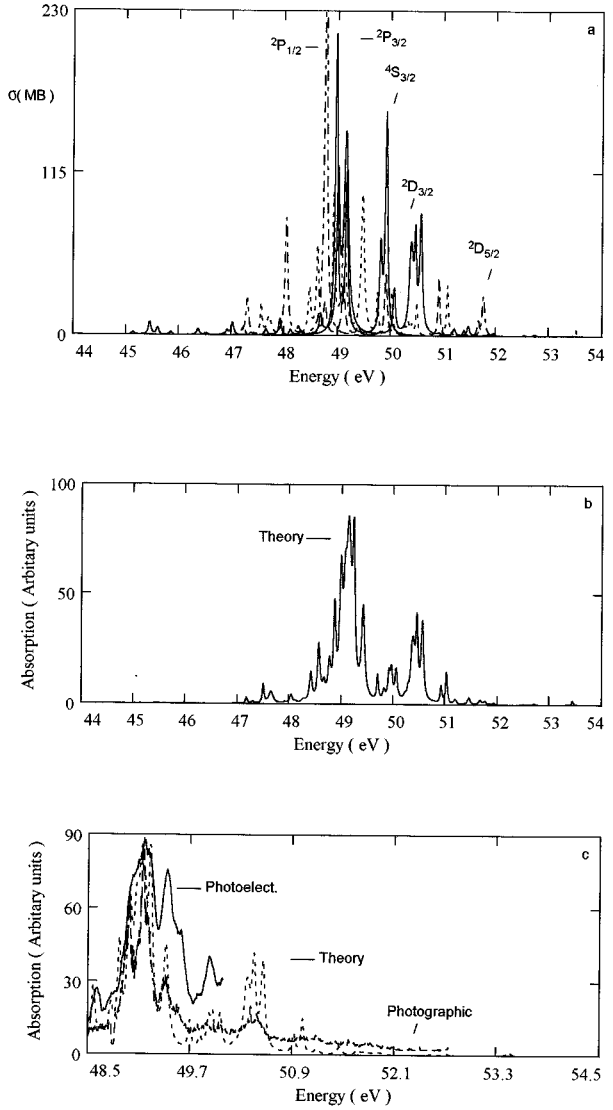

FIG. 3. (a) Theoretical contributions due to the individual terms of the $4d^{10}5s^25p^3$ configuration to the $4d\rightarrow 5p$ photoabsorption cross section of I^{2+}. (b) Relative contributions of the individual terms weighted as expected for a 2-eV plasma and summed. (c) Comparison between theoretical and experimental spectra.

dal centrifugal potential, are essentially hydrogenic, and have effectively zero overlap with the $4d$ core function and $\langle nf|r|4d\rangle \cong 0$. In the case of neutral iodine the resonance was found to peak at 91 or 34 eV above threshold, have a full width at half maximum (FWHM) of 38 eV, and a maximum cross section of 6.5 Mb [8]. Theoretical calculations by Combet-Farnoux and Ben Amar [26] performed in an LS coupling scheme using the coupled-channels method [27] give a description of the $4d$ photoabsorption which is almost identical to that of xenon. For xenon the $4d\rightarrow \varepsilon f$ maximum occurs 32 eV above threshold, has a cross section of 22 Mb, and has a FWHM of 39 eV [28], all of which have been reproduced almost exactly by theory [29] when multielectron processes, core relaxation, and intershell coupling effects are allowed for. In contrast, the predicted cross section of iodine, 30 Mb, is much larger than the experimental one. The anomalously low value of the integrated oscillator strength

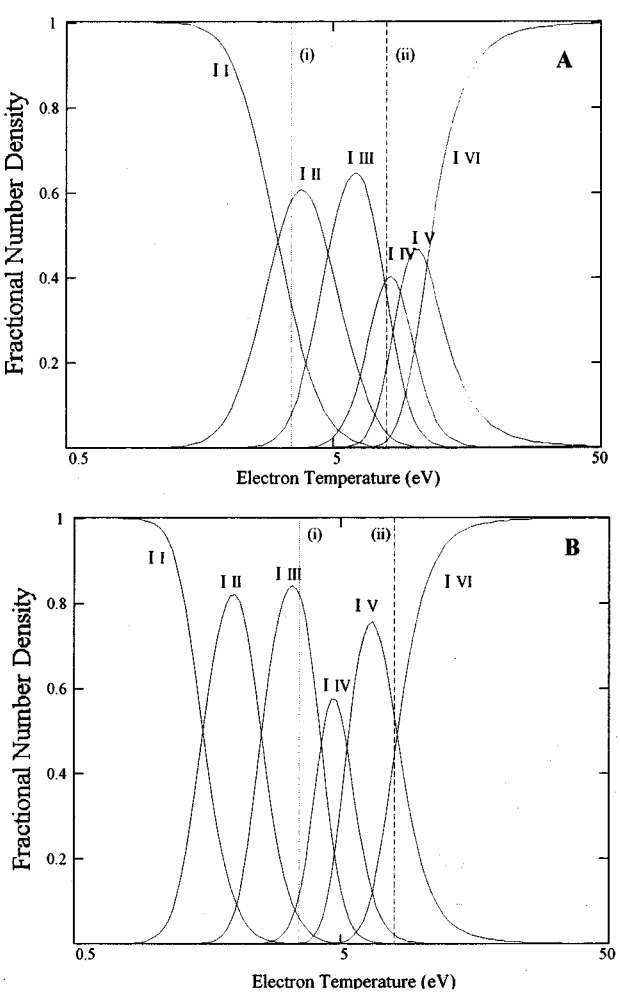

FIG. 4. Ion stage distributions for different values of electron temperature in an iodine plasma at electron densities of 2×10^{21} cm^{-3} (top) and 1×10^{19} cm^{-3} (bottom). (i) Conditions of photographic experiment. (ii) Conditions of photoelectric experiment.

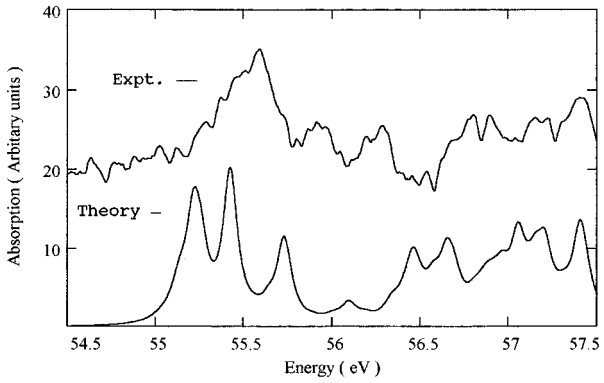

FIG. 5. Comparison between theory and experiment for the $4d\rightarrow 6p$, $7p$, etc., transitions in neutral iodine. Note the spectra agree best if the theoretical spectrum is shifted by ~ 0.15 eV towards higher energy.

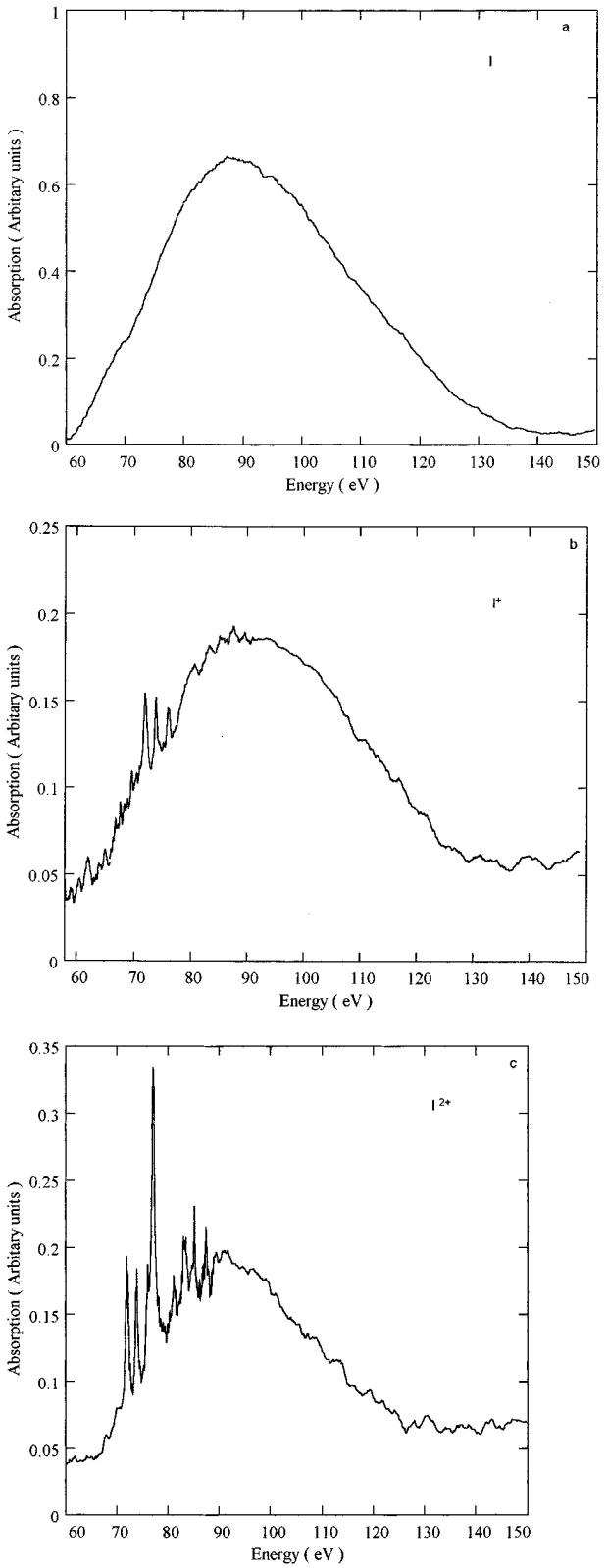

FIG. 6. Experimental spectra of (a) neutral iodine, (b) I^+, and (c) I^{2+} in the $4d \rightarrow \varepsilon f$ region recorded with the photoelectronic detection system. Note that the spectrum in (c) contains contributions from I^+ and I^{3+} also (see text).

of the iodine resonance by comparison with xenon, cesium, barium, and the lower-Z lanthanides has also been noted from studies on I_2 [13] and CH_3I [30,31], where absorption in the 90-eV region is completely dominated by the iodine $4d$ electrons. In the present work, spectra were recorded using the electronic detection system at interlaser time delays of 50, 120, and 400 ns (Fig. 6). The longest time delay yielded a spectrum of neutral iodine with a peak at approximately 88 eV and a FWHM close to 35 eV [Fig. 6(a)]. Any minor differences between this profile and that deduced by Nahon *et al.* [8] can be attributed to the presence here of photoexcitation from the $5s^2 5p^5\ ^2P_{1/2}$ as well as the ground $^2P_{3/2}$. An attempt to calculate the $4d$-εf and εp continuum cross section was made using the Cowan code. Continuum radial wave functions for a range of εl energies from 3 to 50 eV were derived and the $\langle 4d(r)|r|\varepsilon l(r)\rangle$ matrix elements were evaluated. From these, the continuum photoionization cross sections can be calculated since [29]

$$\sigma(4d \rightarrow \varepsilon f) = 8\pi\alpha a_0^2 (\varepsilon - \varepsilon_{4d}) |\langle 4d|r|\varepsilon f\rangle|^2,$$

$$\sigma(4d - \varepsilon p) = \tfrac{16\pi}{3} \alpha a_0^2 (\varepsilon - \varepsilon_{4d}) |\langle 4d|r|\varepsilon p\rangle|^2,$$

where $\varepsilon - \varepsilon_{4d}$ is the energy required to produce an electron with kinetic energy ε by $4d$ photoexcitation. The predicted peak lies at 60 eV, compared with the earlier calculated value of 100 eV [26]. The maximum predicted value for the $4d \rightarrow \varepsilon f$ cross section is predicted as 48 Mb, which is too large, and the resonance profile is too narrow. These results are consistent with other theoretical predictions based on single-particle models [32].

Since giant dipole resonances or shape resonances in the spectra of atoms and ions can be considered to be collective phenomena [33] where sharing of the excitation energy (and cooperative effects) can be invoked to describe their characteristic shapes a theoretical description must inherently be many-body in nature. Two such theoretical prescriptions are many-body perturbation theory [34] and the random-phase approximation with exchange [35]. Both have yielded significant insights into the origin and unique features of $4d - \varepsilon f$ resonances. Yet another approach is the time-dependent local-density approximation (TDLDA) as discussed by Zangwill and Soven [36]. The underlying idea is that the external electromagnetic field causes a time-dependent polarization of the atomic-charge cloud resulting in an induced electromagnetic field. External and induced fields superimpose to yield an effective driving field to which the electrons responds independently. The photoabsorption cross section $\sigma(\omega)$ is then obtained from the frequency-dependent atomic polarizability $\alpha(\omega)$ using $\sigma(\omega) = 4\pi(\omega/c)\mathrm{Im}[\alpha(\omega)]$. In our second set of calculations photoabsorption cross sections for atomic iodine and a number of its ions have been computed using the relativistic and nonrelativistic TDLDA codes DAVID [37] and GOLIATH [38]. Following the lead given by Nuroh *et al.* [39] for the Ba isonuclear sequence, we have made preliminary studies of the effect of increasing ionization on the $4d \rightarrow f$ channel along the iodine isonuclear sequence. For neutral iodine a nonrelativistic calculation places the $4d \rightarrow \varepsilon f$ peak at 96 eV and again overestimates the cross-section maximum as 27 Mb. The results of both these calculations are shown in Fig. 7, where they are compared directly to the experimental spectrum whose profile has been adjusted to agree with the previous experimentally derived peak [8]. Since the effective number of electrons participating in the photoabsorption pro-

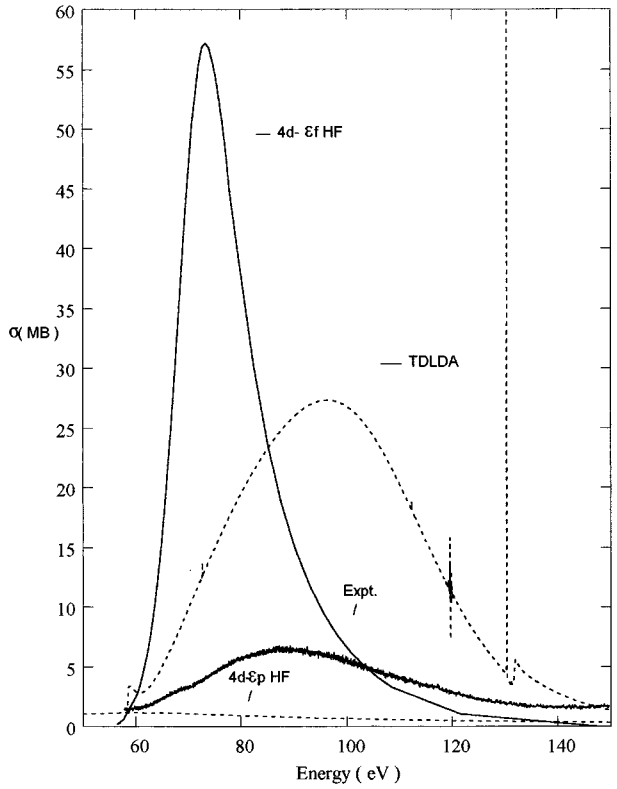

FIG. 7. Comparison between the experimental $4d\rightarrow\varepsilon f$ spectrum of neutral iodine and the results of Hartree-Fock and TDLDA calculations. The experimental curve is fitted to the absolute cross section data of Nahon *et al.* [8].

cess is $N_{\text{eff}}=\int(df/d\varepsilon)d\varepsilon$, Nahon *et al.* [8] deduced a value of $N_{\text{eff}}=3.2$ for the iodine shape resonance from their photoelectron spectrum. For Xe and Te, by comparison, $N_{\text{eff}}=11$ and 9, respectively [40], so the anomalously low cross section cannot be solely due to the open $5p$ subshell. In the case of molecules and clusters environmental factors which conspire to produce strong symmetry effects can reduce continuum cross sections. It is known, for example, that the $4d\rightarrow\varepsilon f$ resonance is predicted to be considerably reduced in Xe or Ba atoms trapped at the center of fullerene molecules [41]. In this reference the carbon atoms were modeled using time-dependent density-functional theory, which is essentially equivalent to TDLDA, as constituting a rigid electropositive spherically symmetric jellium shell whose presence causes the appearance of additional nodes in the wave functions of the scattering states which must be orthogonal to two bound f states of the jellium electron distribution. Since no such effects are plausible in an atomic system the origin of the discrepancy must remain unclear.

2. Singly ionized iodine

In Fig. 6(b) the spectrum recorded at an interlaser time delay of 120 ns is seen to contain three well-resolved peaks at 71.68, 73.81, and 75.84 eV as well as other structures extending downwards to 60 eV. Since $4d$-$5p$ transition in I^+ are observed under these conditions, these features are attributed to I^+ and the spectrum is a mixture of I and I^+. The earlier Cowan code calculations with the extended excited-state basis predict that strong lines should be observed in the 60–70-eV region as a result of $4d^{10}5s^25p^4\rightarrow 4d^95s^25p^4nf$ excitation. The individual $4d^9nf$ terms are so highly mixed in the basis used that the choice of n is rather arbitrary. The importance of such hybridization was first noted in an early theoretical work on Ba^{2+} [42]. The lines do indeed form into a number of relatively sharp features when transitions from the differing ground configurations terms are summed using the same ratios as best reproduced the $4d\rightarrow 5p$ profiles. However, they appear to be shifted downwards by 10 eV in energy. The TDLDA calculations also predict some discrete structure near 66 eV with a strong peak dominating the continuum cross section at 96 eV. The experimental value for this peak is 89 eV. The results of both of these calculations are presented in Fig. 8, where they can be compared directly with the experimental profile. In particular the TDLDA gives a very good fit to the observed spectrum above 100 eV. The cross section of the TDLDA spectrum is again questionable in view of the situation for neutral iodine.

3. Doubly ionized iodine

In the spectrum of Fig. 6(c) recorded at the shortest time delay the I^+ features are still evident but additional strong lines appear due to photoabsorption in higher stages. Indeed, this behavior bears a striking similarity to observed change in the $4d\rightarrow nf,\varepsilon f$ cross section in progressing from Ba to Ba^{2+}, [42,43] which along with lanthanum is the only element for which f wave collapse with increasing ionization has been studied experimentally. In Ba^{2+} there is still considerable continuum absorption but a major part of the oscillator strength has shifted into the bound region. It has been interpreted as arising from the collapse of the $4f$ wave function from the outer well, where it is an eigenstate in neutral barium, to the core region as the centrifugal barrier decreases with increasing ionization and the $\langle 4d|r|nf\rangle$ dipole-matrix elements increase as a consequence. With increasing ionization the calculations predict that the oscillator strength will eventually concentrate in the $4d^{10}\rightarrow 4d^94f(^1P_1)$ transition [44,45] since the centrifugal barrier disappears, the $l=3$ potential well becomes deeper and narrower and the nf levels separate in energy. In the Ba^{2+} spectrum four lines of almost equal intensity are observed. The theoretical approach that agrees best with observation has been reported by Clarke [46], who used a multiconfiguration intermediate coupling HF calculation with some correlation in the initial and final states and identified the strongest lines as $4d^{10}\rightarrow 4d^94f,5f,6f$, and $7f\ ^1P_1$ transitions. Subsequently Hansen *et al.* [47] showed that the sharpness of the features is a consequence of the fact that the $4f$ orbital is only partially collapsed in the $4f\ ^1P$ state, and that in the isoelectronic ion La^{3+} where the $4f\ ^1P$ is collapsed the autoionization width is of the order of 1–2 eV. The nonradiative relaxation of the $4d$ hole leading to $5p$ autoionization is determined by the electrostatic $R^k(4f5p,4d\varepsilon l)$ integral whose magnitude depends on the degree of $4f$ collapse. More recently, the linewidth of the $4d^94f\ ^1P$ state has been determined experimentally as approximately 2.0 eV [48].

The Cowan code calculations performed for the $4d^{10}5s^25p^3\rightarrow 4d^95s^25p^3(np+mf+\varepsilon p+\varepsilon f)$ excitations which were used to interpret the $4d\rightarrow 5p$ data predict the

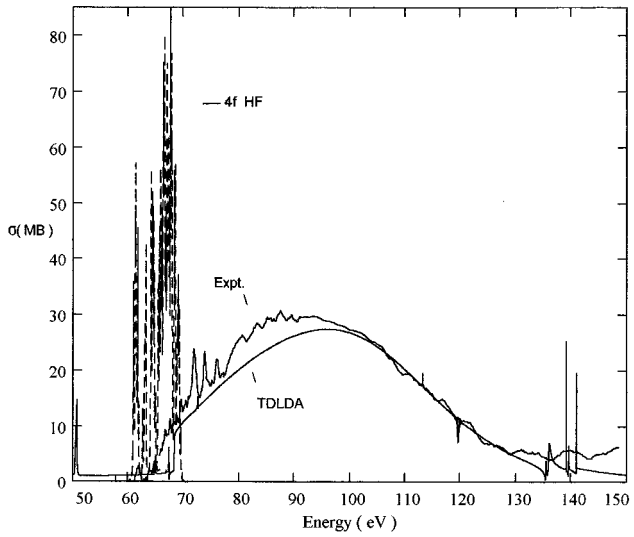

FIG. 8. Comparison between the experimental $4d \rightarrow nf,\ \varepsilon f$ spectrum of I^{2+} and the results of HF (discrete spectrum) and TDLDA calculations. The experimental spectrum was arbitrarily fitted to give best agreement with the TDLDA results.

existence of a single intense feature near 82 eV. Moreover, the presence of absorption from excited terms of the ground configuration only extends the width of this feature by approximately 0.4 eV and gives no additional strong lines. The strongest contributing transitions along with their positions and gf values are listed in Table X while their population weighted sum is shown in Fig. 9. In constructing this figure the autoionizing linewidths were not explicitly calculated but each line is given an artificial linewidth of 0.25 eV in order to compare with experimental data. Moreover, the validity of such theoretical data is questionable since, as already pointed out, the shakeoff probability is known to increase as the $4d^{-1}$ limit is approached and has been shown by Nagata *et al.* [49] to be responsible for approximately 33% of the total nonradiative decay at the higher energy end of the $4d \rightarrow nf$ region in cesium. It should also be noted that the nf LS term labels used in Table X correspond to leading eigenvectors in each case and is strongly dependent on the choice of basis used. In the case cited, bound nf states up to $n=10$ were implicitly included. Increasing the basis set up to $m=16$ led to a new set of labels and also shifted the feature towards higher energy. However, the overall profile was unaffected and in particular no additional structure was predicted to lie on the high-energy side in any of these calculations. Based on all of these data we associate the intense single feature at 77.2 eV with discrete $4d \rightarrow f$ absorption in I^{2+}. Its sharpness indicates that the $4f$ wave function is again only partially collapsed in I^{2+}. This conclusion is strongly borne out by the TDLDA results, which show a strong shape resonance peaking at 96 eV as before with an intense single feature at 78.7 eV, which almost coincides with observation and some weaker discrete structure between 70 and 76 eV (Fig. 9), so even at I^{2+} the *ab initio* many-body predictions are more accurate.

D. Higher ion stages

The assignment of the intense feature at 77.5 eV to I^{2+} leaves the problem of identifying the remaining features at 81.2., 83.2, 85.3, and 87.3 eV. The nonrelativistic TDLDA calculation for I^{3+} (Fig. 10) predicts three intense resonances close to 79.5, 85, and 87 eV. Because of their enormous oscillator strength only a tiny population of I^{3+}, too small to lead to any detectable $4d \rightarrow 5p$ transitions, would be sufficient to observe these features. The calculations also predict a large cross section ($\sim$24 Mb) for $4d \rightarrow \varepsilon f$ transitions at the $4d^{-1}$ threshold. In I^{4+}, the TDLDA calculations predict that an intense single feature should be observed at 102 eV and the continuum cross section is still high at threshold, indicating that the $4f$ state is not yet fully localized in the core region as the transfer of oscillator strength from εf to $4f$ which should accompany $4f$ collapse is not yet complete. At I^{7+} the entire nf series become bound nonautoionizing states and further calculations show that the $4d \rightarrow \varepsilon f$ cross section is finally reduced to a value of a few Mb at this point and the spectrum becomes more ''single-particle'' in nature. This behavior is consistent with that already reported for $4d \rightarrow 4f$ transitions in Xe. The transfer of oscillator strength to the $4d \rightarrow 4f$ transition is essentially complete at Xe^{8+} and the gf value essentially stabilizes past this stage [50].

IV. CONCLUSION

The $4d$ photoabsorption spectra of I, I^{+}, and I^{2+} have been observed in the 45–150-eV spectral region using the DLP technique. Calculations with the Cowan suite of programs were successful in accounting for all of the observed discrete structure which arises from $4d \rightarrow 5p$ transitions at the low-energy end and $4d \rightarrow nf$ transitions occurring just below the $4d$ threshold in I^{+} and I^{2+}. $4d \rightarrow 6p$ lines of I

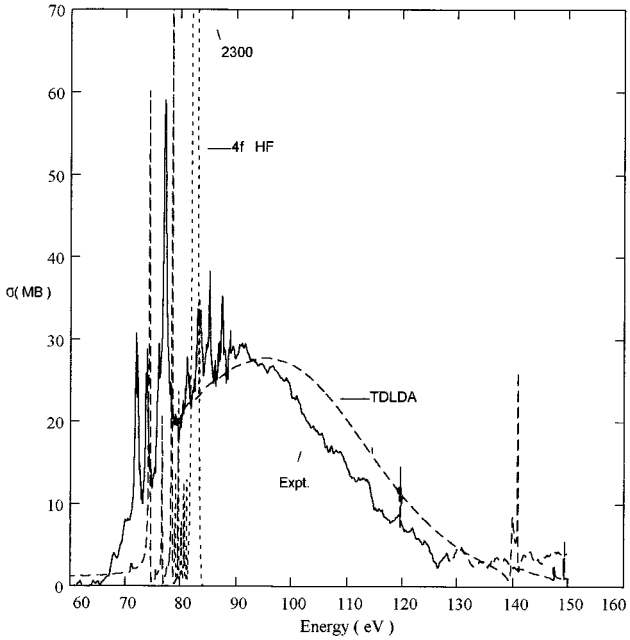

FIG. 9. Comparison between the experimental $4d \rightarrow nf,\ \varepsilon f$ spectrum of I^{2+} and the results of HF (discrete spectrum) and TDLDA calculations. The experimental spectrum was arbitrarily fitted to give best agreement with the TDLDA results. It should be noted that the experimental spectrum also contains some contributions from I^{+} and I^{3+}.

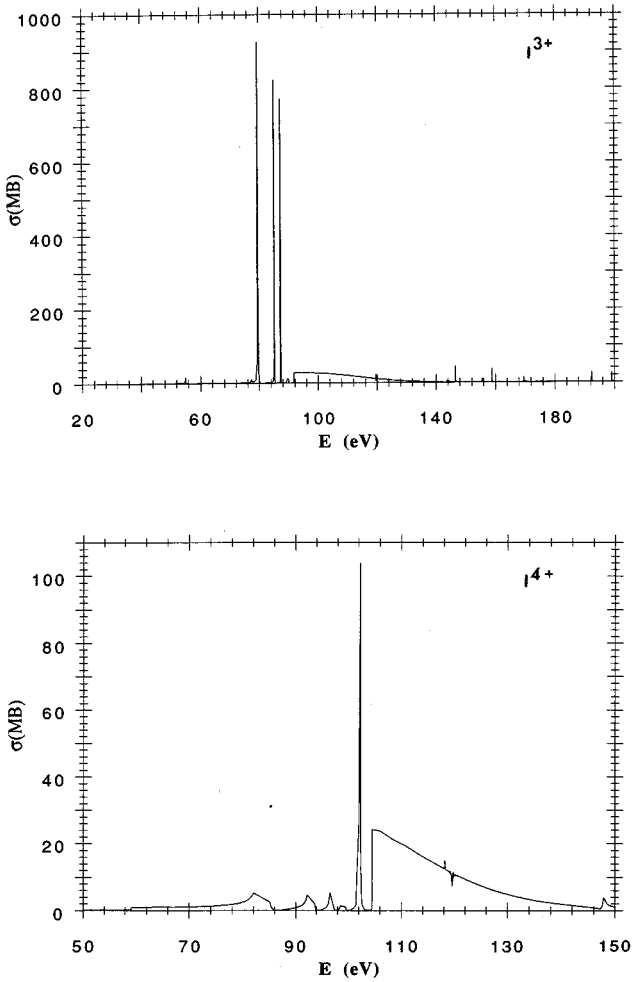

FIG. 10. $4d \rightarrow nf,\ \varepsilon f$ spectra for I^{3+} and I^{4+} calculated using the nonrelativistic TDLDA method.

and I^{+} were also identified. The most striking difference in the spectra arise not from the opening of the $5p$ subshell but from the gradual collapse of the $4f$ wave function which causes the $4d \rightarrow f$ oscillator strength to shift slowly from a shape resonance in the neutral to the discrete spectrum in the ions. TDLDA calculations with the Zangwill and Liberman codes successfully reproduced this behavior. In each case the features observed could be accounted for by assuming absorption from the ground and lowest excited states.

TABLE X. Strongest (gf) transitions responsible for the intense $4d \rightarrow f$ resonance feature observed at 77.2 eV in the I^{2+} spectrum. The excited-state basis contained nf states from $n=4$ to $n=10$.

Transition	E_{HF} (eV)	gf
$^4S_{3/2} \rightarrow 9f(^2P)^2F_{3/2}$	82.023	1.588
$4f(^4S)^4P_{3/2}$	82.098	2.841
$8f(^2P)^4D_{5/2}$	82.102	1.034
$10f(^2P)^4P_{1/2}$	82.106	1.671
$9f(^2D)^2P_{3/2}$	82.109	1.414
$8f(^2P)^2F_{5/2}$	82.114	3.386
$9f(^2D)^2D_{5/2}$	82.138	1.281
$10f(^2P)^4P_{3/2}$	82.170	1.10
$10f(^2P)^4D_{5/2}$	82.179	1.559
$^2D_{3/2} \rightarrow 9f(^2P)^4G_{5/2}$	82.105	1.185
$10f(^2P)^2F_{5/2}$	82.148	1.873
$9f(^2P)^2P_{3/2}$	82.216	3.708
$9f(^2P)^2D_{3/2}$	82.237	2.146
$4f(^2D)^2F_{5/2}$	82.316	5.233
$5f(^2D)^2P_{1/2}$	82.379	3.478
$^2D_{5/2} \rightarrow 4f(^2D)^2D_{5/2}$	82.399	8.863
$5f(^2D)^2P_{3/2}$	82.416	6.850
$^2P_{1/2} \rightarrow 6f(^2P)^2D_{3/2}$	82.414	6.905
$^2P_{3/2} \rightarrow 5f(^2P)^2P_{3/2}$	82.715	7.213
$5f(^2P)^2S_{1/2}$	82.561	3.479
$6f(^2P)^2D_{5/2}$	82.559	10.512

ACKNOWLEDGMENTS

This work was supported by the Irish Science and Technology agency FORBAIRT under research Grants Nos. SC-93-144, SC-93-154, and SC-95-403 and the European Union under HCM Contract No. CHRX-CT93-0361. The assistance of Professor M.W.D. Mansfield of University College Cork in obtaining the microdensitometer traces used for constructing Figs. 2 and 3 is gratefully acknowledged.

[1] P. K. Carroll and E. T. Kennedy, Phys. Rev. Lett. **38**, 1068 (1977).
[2] J. T. Costello, E. T. Kennedy, B. F. Sonntag, and C. Cromer, J. Phys. B **24**, 5063 (1991).
[3] M. Pettini, M. Mazzoni, and G. P. Tozzi, Phys. Lett. **82**, 168 (1981).
[4] J. Tremblay, M. Larzilliere, F. Combet-Farnoux, and P. Morin, Phys. Rev. A **38**, 3804 (1988).
[5] M. Meyer, J. Lacoursière, P. Morin, and F. Combet-Farnoux, J. Phys. B **27**, 3875 (1994).
[6] L. Nahon, L. Duffy, P. Morin, F. Combet-Farnoux, J. Tremblay, and M. Larzilliere, Phys. Rev. A **41**, 4879 (1990).
[7] L. Nahon and P. Morin, Phys. Rev. A **45**, 2887 (1992).
[8] L. Nahon, A. Svensson, and P. Morin, Phys. Rev. A **43**, 2328 (1991).
[9] U. Becker, T. Prescher, E. Schmidt, B. Sonntag, and H. E. Wetzel, Phys. Rev. A **33**, 3891 (1986).
[10] For details see *Giant Resonances in Atoms, Molecules and Solids*, edited by J. P. Connerade, J. M. Estava, and R. C. Karnatak (Plenum, New York, 1987).
[11] G. O'Sullivan, P. K. Carroll, J. Conway, P. Dunne, R. Faulkner, T. McCormack, C. McGuinness, P. van Kampen, and B. Weinmann, Opt. Eng. **33**, 3993 (1994).
[12] E. T. Kennedy, J. T. Costello, J. P. Mosnier, A. A. Cafolla, M. Collins, L. Kiernan, U. Köble, M. H. Sayyad, M. Shaw, B. F. Sonntag, and R. Barchewitz, Opt. Eng. **33**, 3984 (1994).

[13] F. J. Comes, U. Nielsen, and W. H. E. Schwartz, J. Chem. Phys. **58**, 2230 (1973).
[14] R. D. Cowan, *The Theory of Atomic Structure and Spectra* (University of California Press, Berkeley, 1981).
[15] L. Nahon, P. Morin, and F. Combet-Farnoux, Phys. Scr. **T41**, 104 (1992).
[16] S. Southworth, U. Becker, C. M. Truesdale, P. H. Kobrin, D. W. Lindle, S. Owaki, and D. A. Shirley, Phys. Rev. A **28**, 261 (1983).
[17] H. Aksela, S. Aksela, S. Bancroft, and K. H. Tan, Phys. Rev. A **33**, 3867 (1986).
[18] H. Aksela, S. Aksela, and H. Pulkkinen, Phys. Rev. A **30**, 865 (1984).
[19] J. Berkowitz and G. L. Goodman, J. Chem. Phys. **71**, 1754 (1979).
[20] J. Sugar, Phys. Rev. B **5**, 1785 (1972).
[21] D. F. Colombant and G. F. Tonon, J. Appl. Phys. **44**, 3524 (1973).
[22] F. Combet-Farnoux, Phys. Scr. **T41**, 28 (1992).
[23] G. C. King, M. Tronc, F. H. Read, and R. C. Bradford, J. Phys. B **10**, 2479 (1977).
[24] U. Fano and J. W. Cooper, Phys. Rev. **137**, A1364 (1965).
[25] T. Hayashi, Y. Morioka, Y. Kageyama, M. Watanabe, I. H. Suzuki, A. Mikuni, G. Isoyama, S. Asoaka, and M. Nakumura, J. Phys. B **17**, 1511 (1989).
[26] F. Combet-Farnoux and M. Ben Aymar, J. Electron Spectrosc. Relat. Phenom. **41**, 67 (1986).
[27] M. Ben Aymar and F. Combet-Farnoux, J. Phys. B **16**, 2339 (1983).
[28] B. Kammerling, H. Kossmon, and V. Schmidt, J. Phys. B **22**, 841 (1989).
[29] M. Ya. Amusia, L. V. Chernysheva, G. F. Gribakin, and K. L. Tsemekhman, J. Phys. B **23**, 393 (1990).
[30] D. W. Lindle, P. H. Kobrin, C. U. Truesdale, T. A. Ferret, P. A. Heinmann, H. G. Kerkhoff, U. Becker, and D. A. Shirley, Phys. Rev. A **30**, 239 (1984).
[31] G. O'Sullivan, J. Phys. B **15**, L327 (1982).
[32] S. T. Manson and J. W. Cooper, Phys. Rev. **165**, 126 (1968).
[33] G. Wendin, Phys. Lett. **46A**, 119 (1973).
[34] H. P. Kelly, Phys. Scr. **T17**, 109 (1987).
[35] M. Ya. Amusia, V. K. Ivanov, and V. A. Kupchenko, Z. Phys. D **14**, 210 (1989).
[36] A. Zangwill and P. Soven, Phys. Rev. A **21**, 1561 (1980).
[37] D. A. Liberman and A. Zangwill, Comput. Phys. Commun. **32**, 74 (1984).
[38] A. Zangwill and D. A. Liberman, Comput. Phys. Commun. **32**, 63 (1984).
[39] K. Nuroh, M. J. Stott, and Zareba, Phys. Rev. Lett. **49**, 862 (1982).
[40] B. Sonntag, T. Tuomi, and G. Zimmerer, Phys. Status Solidi **58**, 101 (1973).
[41] M. J. Puska and R. M. Nieminen, Phys. Rev. A **47**, 1181 (1993).
[42] J. P. Connerade and M. W. D. Mansfield, Phys. Rev. Lett. **48**, 131 (1982).
[43] T. B. Lucatorto, T. J. McIlrath, J. Sugar, and S. M. Younger, Phys. Rev. Lett. **47**, 1124 (1981).
[44] K. T. Cheng and C. Froese-Fisher, Phys. Rev. A **28**, 2811 (1983).
[45] K. T. Cheng and W. R. Johnson, Phys. Rev. A **28**, 2820 (1983).
[46] C. W. Clark, J. Opt. Soc. Am. B **1**, 626 (1984).
[47] J. E. Hansen, J. Brilly, E. T. Kennedy, and G. O'Sullivan, Phys. Rev. Lett. **63**, 1934 (1989).
[48] U. Köble, L. Kiernan, J. T. Costello, J. P. Mosnier, J. T. Kennedy, V. K. Ivanov, V. A. Kupchenko, and M. S. Shendrik, Phys. Rev. Lett. **74**, 2188 (1995).
[49] T. Nagata, Y. Koh, T. Hayaishi, Y. Hikawa, T. Koizumi, T. Matsuo, Y. Sato, E. Shigemasa, A. Yagishita, and M. Yoshino, J. Phys. B **22**, 3865 (1989).
[50] G. O'Sullivan, J. Phys. B **15**, L765 (1982).